Attached documents

Fig. WP1-1; *Views on the 2nd generation peptide laser printer with 4 from 24 printing units being visible.*

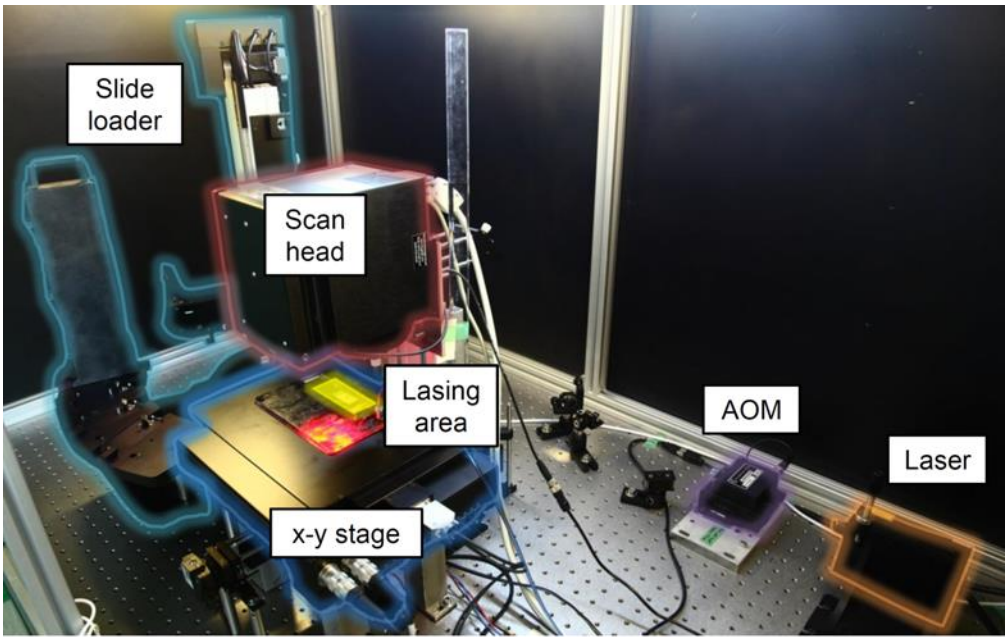

Fig. WP1-2; *Setup of the combinatorial laser-induced forward transfer machine. The laser is modulated by an acousto-optic modulator (AOM) and guided to a scan head system. The laser transfer is conducted on an x-y microscope stage, the lasing area is highlighted in yellow. Donor and acceptor slides are automatically handled and placed by the robotic slide loader.*

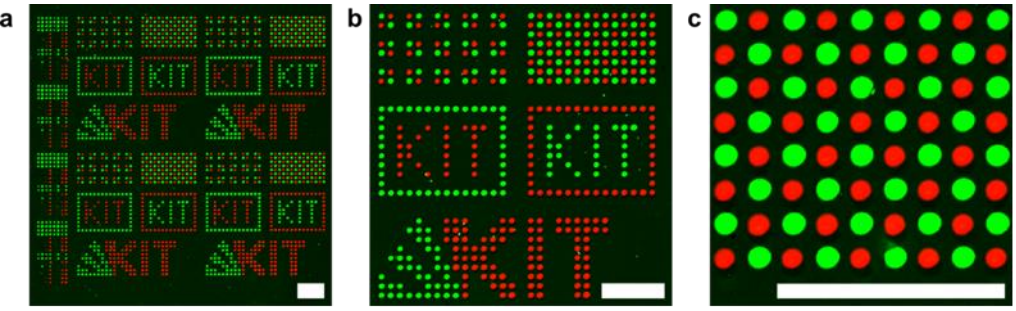

Fig. WP1-4; *Combinatorial synthesis of peptide arrays with cLIFT.* ***(a, b, c)*** *Array containing 64 different peptides with 4,444 peptide spots per cm² (in* ***a*** *and* ***b****) using cLIFT and different donor slides that bear the different amino acid building blocks; scale bars (a) 2 mm, (b) 1 mm, (c) 250 µm. Flag- and HA-peptides were stained with specific anti-Flag and anti-HA antibodies.*

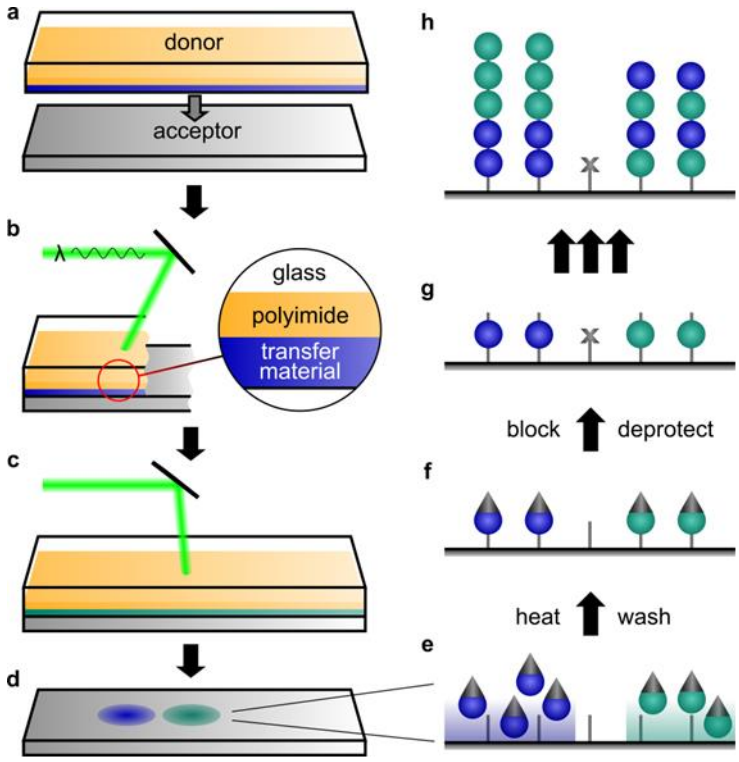

Fig. WP1-3; *Principle of the combinatorial laser-induced forward transfer synthesis. Donor slides bearing different monomer building blocks, embedded in a resin (different colors in (b) and (c)) are positioned on top of an acceptor slide (a). A laser scanning system transfers minute amounts of material to the acceptor slide. Repeating these steps with different donor slides results in a pattern of different amino acid types. The coupling reaction of monomers (e) is initiated by heating the surface. Next, uncoupled amino acid building blocks are removed (f), uncoupled amino groups are blocked, and the protecting groups are removed (g). Repeating the cycle generates in an array of combinatorially synthesized peptides (h).*

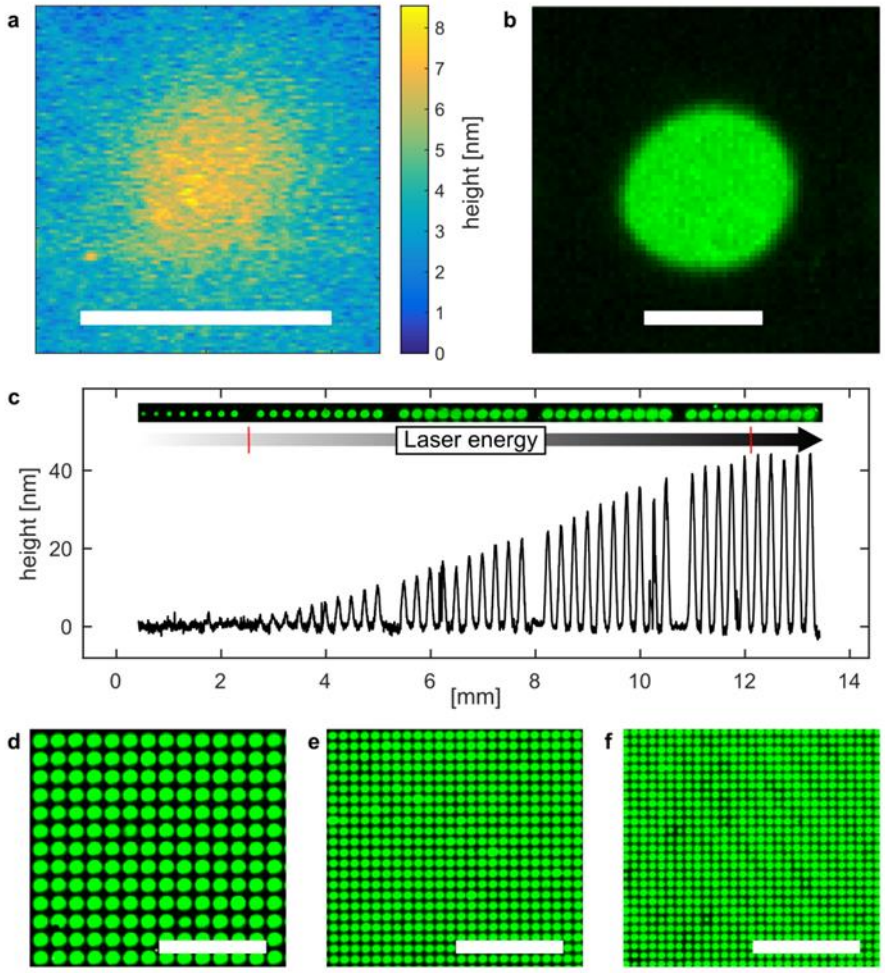

Fig. WP1-6; *Analysis of transferred spots and spot resolution.* ***(a)*** *Topography of the spot with activated leucine monomers in the polymer matrix on the acceptor slide before the coupling and washing steps, measured with phase-shift interferometry. The material spot is approximately 8 nm thick at its center (scale bar 100 µm).* ***(b)*** *The fluorescence image of the spot after coupling of the monomers and staining with a rhodamine dye. The amount of the transferred material is approximately 0.1 ng (scale bar 100 µm).* ***(c)*** *Topography of transferred spot material in dependence of the laser energy. The height of the transferred spot material, containing an activated biotin building block, was measured with phase-shift interferometry, laser energy linearly increases from left to right in steps of 13.6 µJ. The linear correlation of deposited material (1 – 50 nm) and deposited laser energy (450 – 900 µJ) is marked by red lines. The corresponding fluorescence staining pattern of the coupled biotin was obtained with a fluorescently labeled streptavidin.* ***(d-f)*** *Fluorescence images of stained biotin patterns with different pitches:* ***(d)*** *150 µm (4,444 spots/cm²),* ***(e)*** *100 µm (10,000 spots/cm²),* ***(f)*** *75 µm (17,777 spots/cm²).*

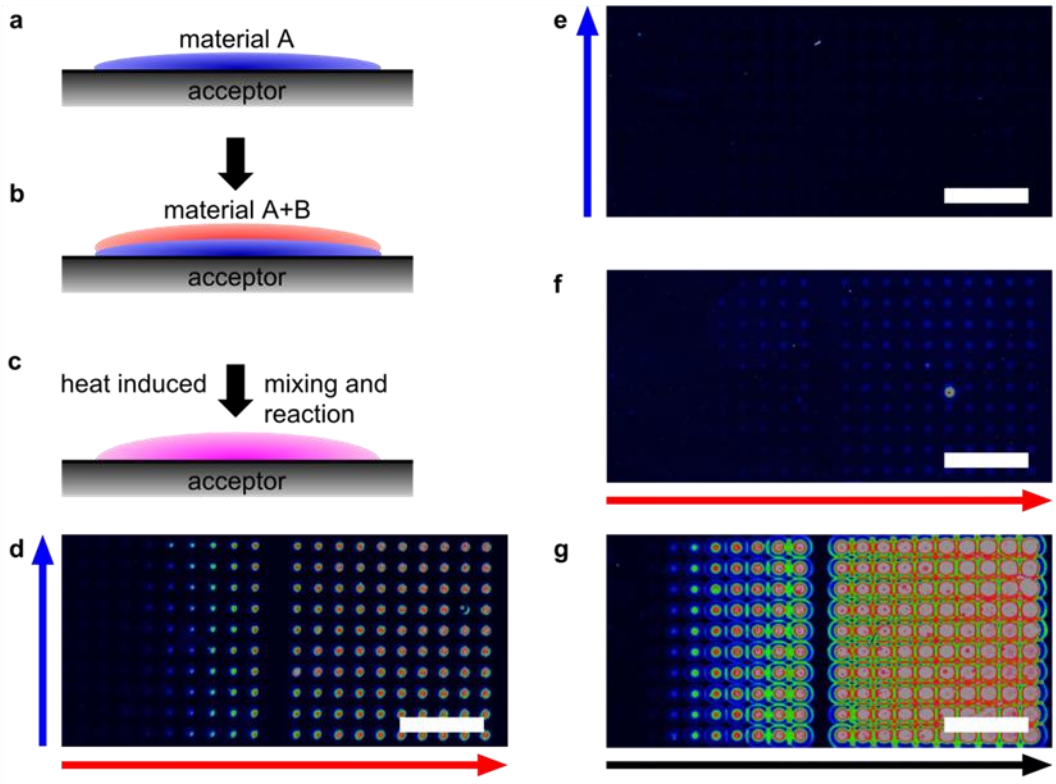

Fig. WP1-7; *Two-step cLIFT gradient patterning experiment for solid phase combinatorial synthesis.* ***(a)*** *Deposition of first material.* ***(b)*** *Deposition of a second material on top of the previous pattern.* ***(c)*** *Heat induced melting of material induces mixing and initiates the reaction.* ***(d-g)*** *Experimental results of an Fmoc-Gly-OH, reacting with DIC and HOBt activation reagents (250 µm pitch); scale bar 1 mm. Free amino groups were stained with a rhodamine dye, illustrated in rainbow colour scale.* ***(d)*** *Two layer reaction of a layer of DIC and HOBt (concentration increases in direction of blue arrow) with a second layer of Fmoc-Gly-OH (concentration increases in direction of red arrow);* ***(e)*** *one layer of DIC and HOBt as a negative control;* ***(f)*** *one layer of Fmoc-Gly-OH as a negative control;* ***(g)*** *one layer of Fmoc-Gly-OPfp as a positive control.*

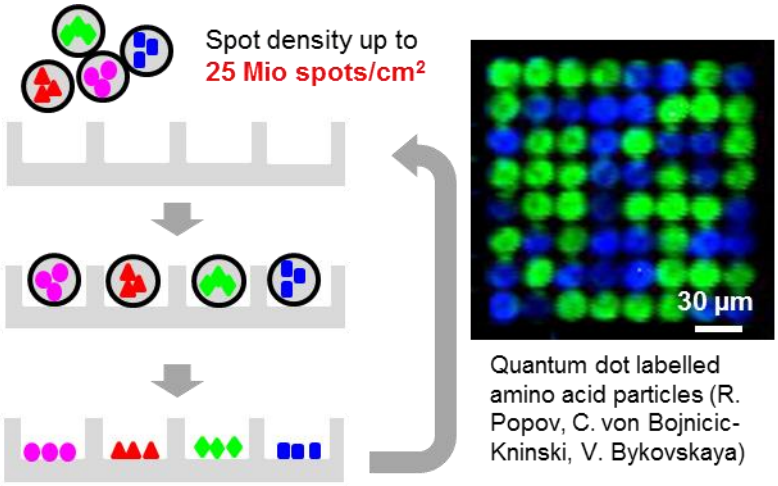

Fig. WP1-8; *One-cavity-one-peptide-method.* ***(left)*** *Differently labelled amino acid particles with narrow size distribution are used to randomly fill micro cavities with exactly one particle per cavity. A fluorescent picture reports which amino acid particle was deposited in the different synthesis sites. Upon melting the activated amino acid diffuses out of the particle and couples to the surface of "its" cavity. Repeating this procedure generates a very high density peptide array.* ***(right)*** *Fluorescent image taken with a CMOS chip that shows two different kinds of amino acid particles at a density of 1 Million per cm².*

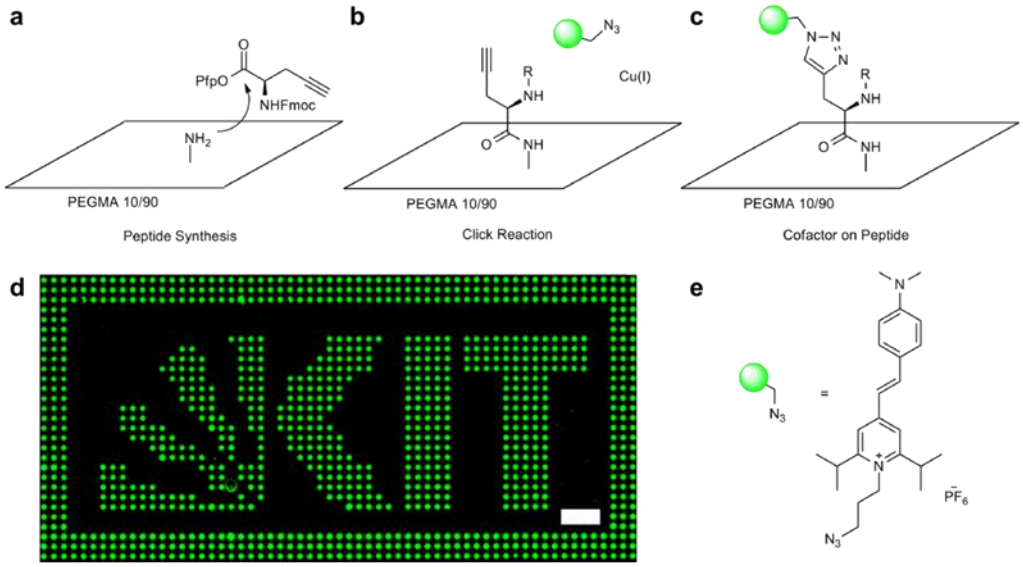

Fig. WP1-9; *Schematic of the click chemistry reaction, using an Fmoc-Pra-OPfp.* ***(a)*** *The synthetic Pra amino acid was patterned and coupled with cLIFT.* ***(b-d)*** *Afterwards, the styrylpyridinium fluorophore from AMU was attached to the Pra in a copper catalyzed click reaction.* ***(e)*** *The fluorescent image of the patterned Pra clicked with the styrylpyridinium fluorophore; spot pitch 250 µm (scale bar 1 mm).*

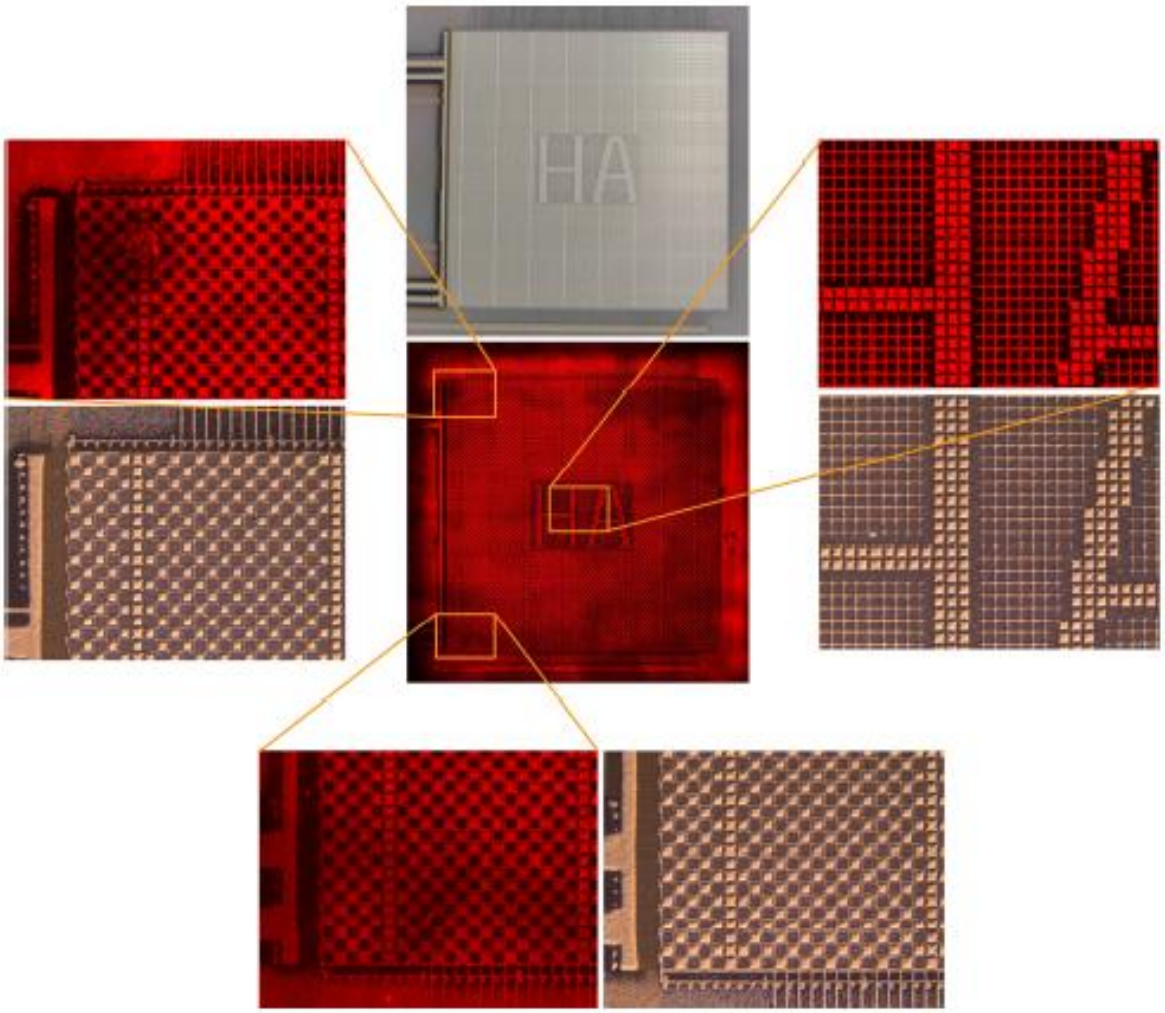

Fig. WP1-11; *Transfer of 10.000 peptides per cm^2 in the array format from a microchip, performed with a transfer time of 20 min, and in 50% TFA in toluene. Greyish pictures show the cystein deposition pattern on the chip while the reddish pictures show the staining of the target membrane with a fluorescently labeled anti-HA antibody. The readout was performed with the GenePix 4000B scanner at 635 nm. Corresponding cysteine particle deposition patterns are compared with immune staining patterns to demonstrate the specificity and (very high) resolution of the transfer. Adjacent pixels have a pitch of ~100µm, the diameter of the grid structures is ~12µm. Lateral diffusion during transfer is estimated to be <2µm.*

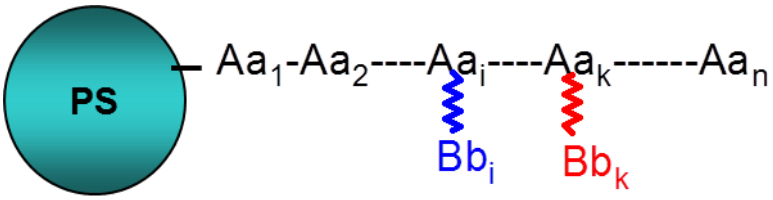

Fig. WP2-1 Insertion of functional building blocks (**Bb**) at various positions in a peptide synthesis on solid support (**PS**).

Fig. WP2-2; *General formulae for **Por-Bb**'s an **Pyr-Bb**'s included in the project. The substituents R and R' can be varied practically at will. The chromophoric system responsible for the photophysical properties is shown with coloured bold bonds. M can be either 2H or various metals such as Zn, Cu, Ni, Mg, Cd, etc. The blue substituents serve to incorporate the Bb's into the peptide chain.*

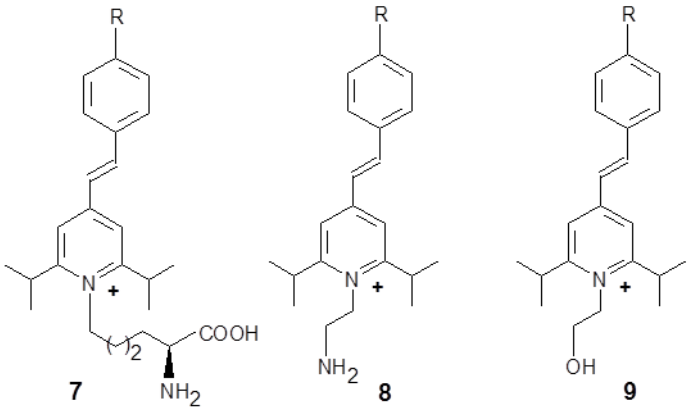

Fig. WP2-4; *Novel styrylpyridinium salts **7-9.** The counteranion can be either hexafluoro-phosphate or tetrafluoroborate.*

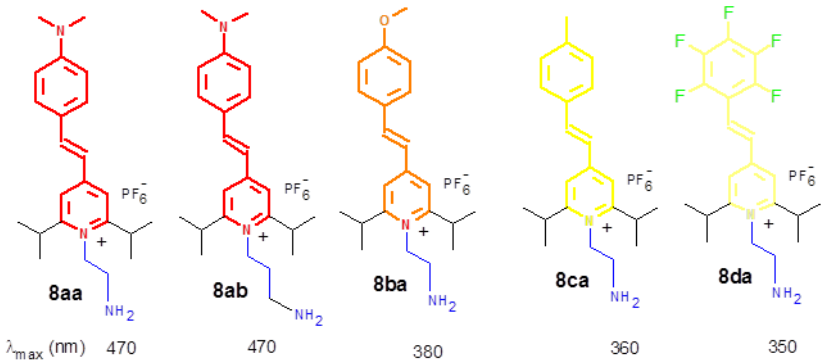

Fig. WP2-8; *Styrylpyridinium compounds fine tuned in their optical properties.*

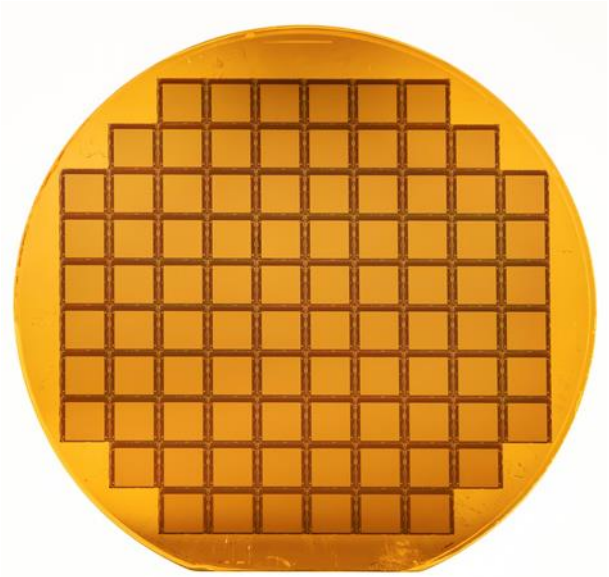

Fig. WP3-2; *150mm wafer containing 88x Measurement Chip 1 after completion of gold add-on process.*

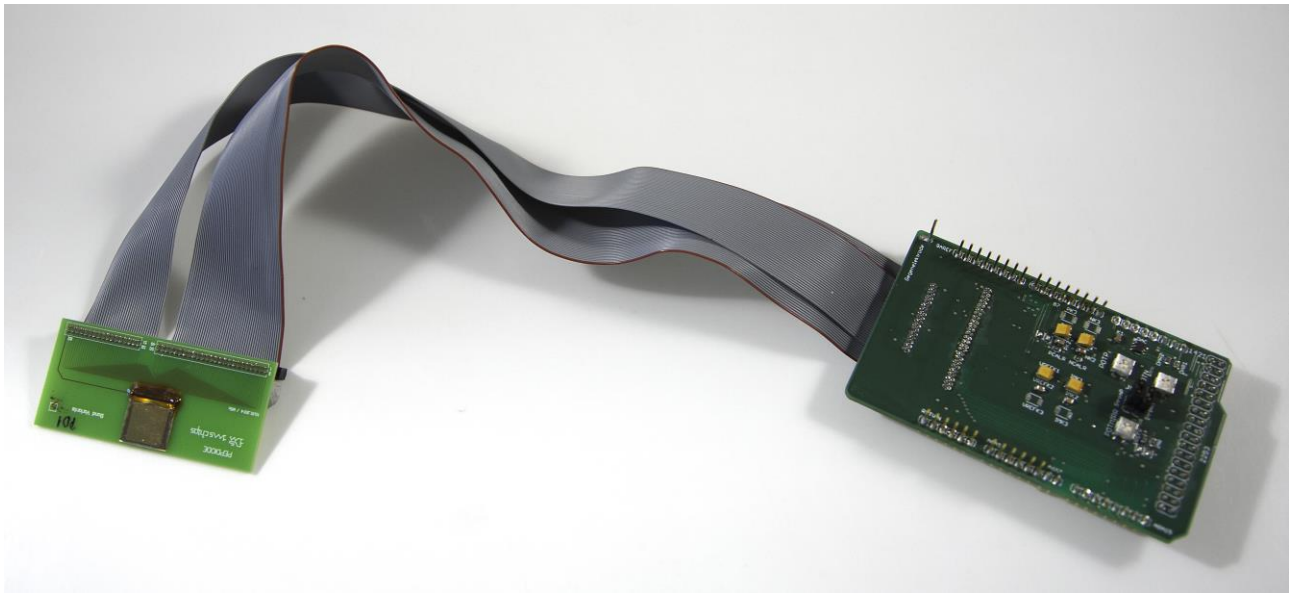

Fig. WP3-4; Arduino shield and connected PCB with Measurement Chip 1

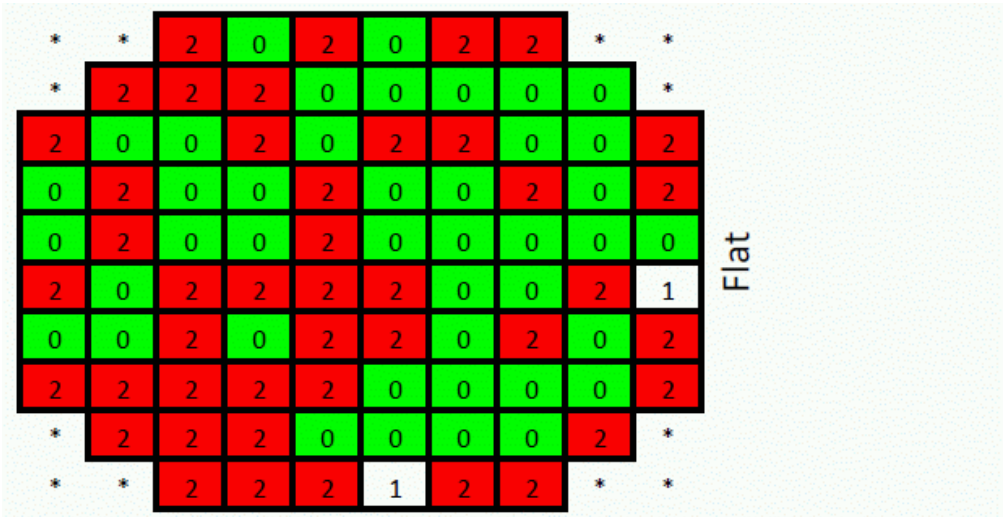

Bin	P_F	Number	Prcnt	Bin_desc
0	PASS	42	48%	Good
1	FAIL	2	2%	CONT
2	FAIL	44	50%	FUNC_Digital

Fig. WP3-5; Wafer test map with a yield of 48%

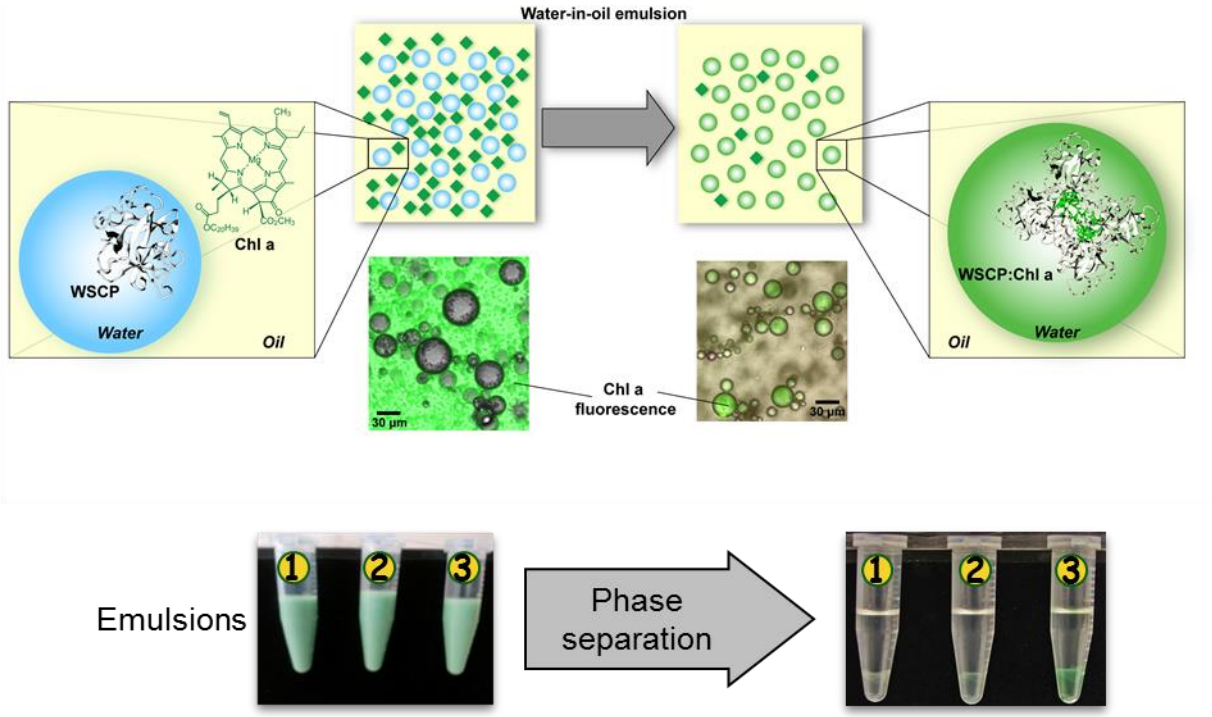

Fig. WP4-1b; *Shown is the enrichment of chlorophyll moieties (from the oil phase) within the water phase, which is induced by an expressed maquette that binds to chlorophyll. (1) E. coli cells, no WSCP plasmid, no induction; (2) E. coli cells, +WSCP plasmid, no induction; (3) E. coli cells, +WSCP plasmid, +induction*

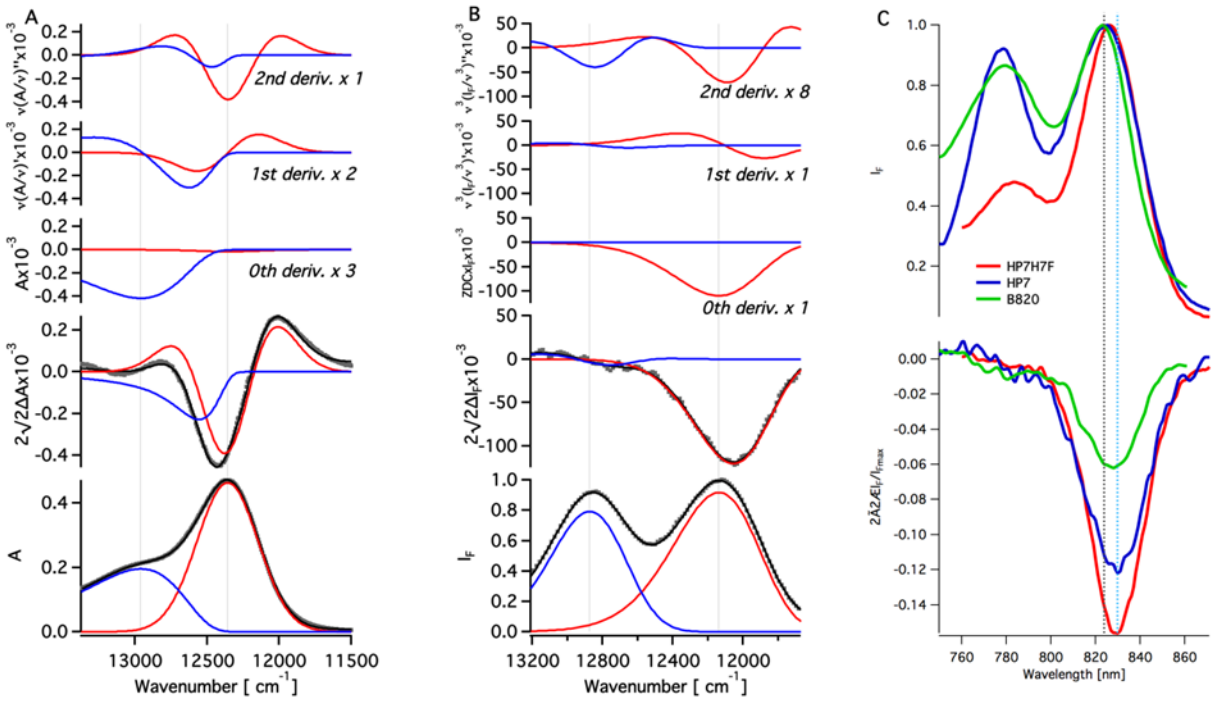

Fig. WP4-1; *Absorbance (A) and Fluorescence (B) spectra and respective Stark spectra and of HP7 ZnBC complex simultaneously fitted with two skewed Gaussian bands shown in red and blue. Experimental data is shown in grey dots, and the fitted curves in solid black lines. The top three graphs present the zero-, first- and second-order derivative components of the SA spectra of each band. For better comparison the Y scale was kept constant and the scaling factors applied to each component are listed on each graph.*

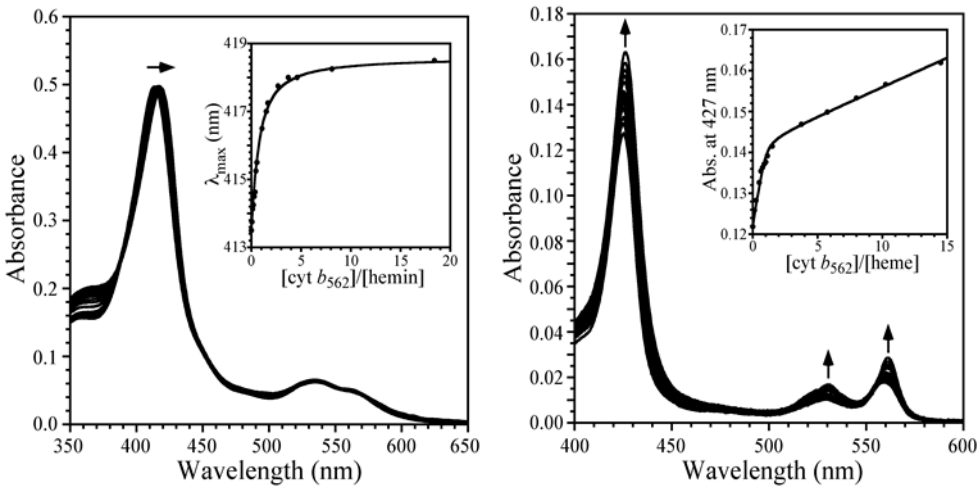

Fig. WP4-2. *Determination of the ferric (left panel) and ferrous (right) heme affinity of cytochrome b562 by competition titration with a de novo designed four helix bundle. The spectral shift in the ferric state, and the increase in molar absorptivity in the ferrous state are fit to competition constants in the insets.*

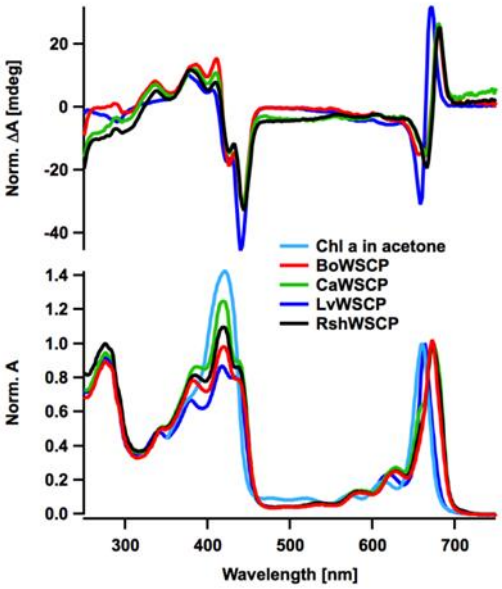

Fig. WP4-3; *CD (top) and absorption spectra (lower part) of Chl complexes of four WSCP variants based on natural WSCP sequences from Brussels sprout (BoWSCP), Cauliflower (CaWSCP), Virginia pepperweed (LvWSCP) and Japanese horseradish (RshWSCP). Absorption and CD spectra were normalized such that the lowest energy Qy absorption peak is unity. The absorption spectrum of Chl in acetone is added for comparison.*

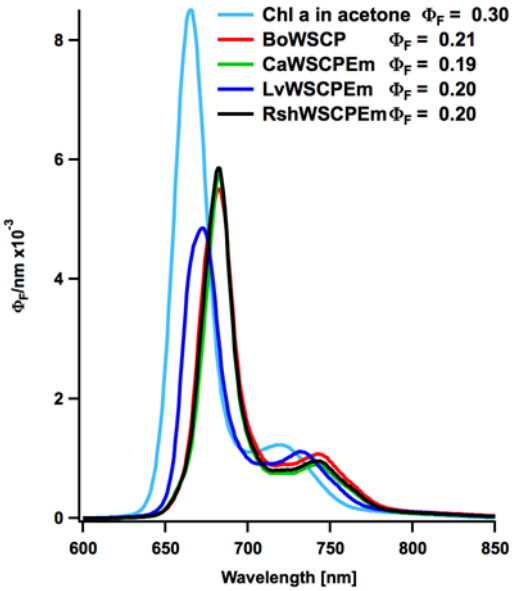

Fig. WP4-4; *Fluorescence emission spectra of Chl complexes of four WSCP variants based on natural WSCP sequences from Brussels sprout (BoWSCP), Cauliflower (CaWSCP), Virginia pepperweed (LvWSCP) and Japanese horseradish (RshWSCP). Absorption and CD spectra were normalized to their actual quantum yield (Φ_F). The emission spectrum of Chl in acetone is added for comparison.*

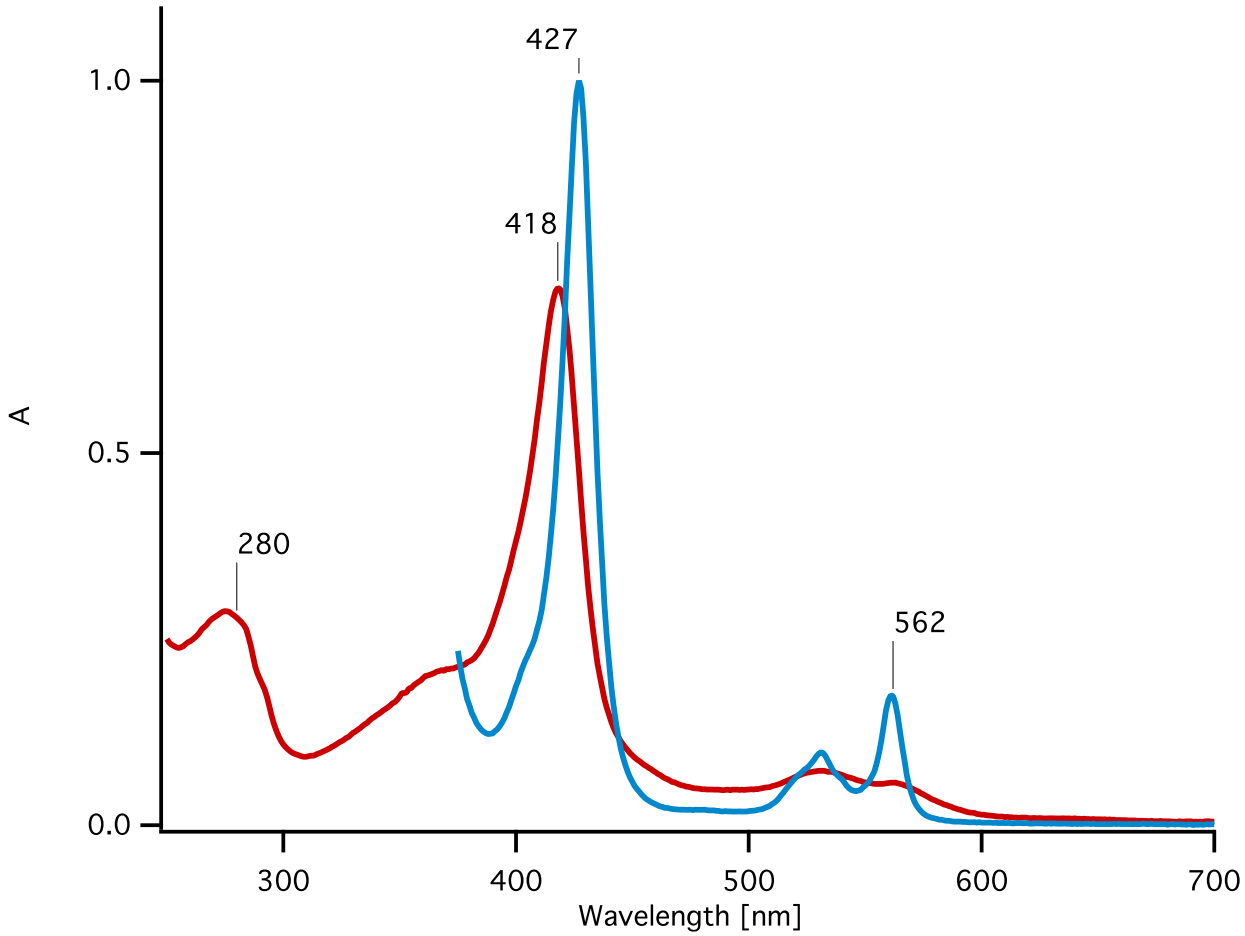

Fig. WP6-1. Absorption spectra of purified Cyt b562::WSCP fusion protein in the presence (blue curve) and absence (red curve) of excess sodium dithionite. Spectra were normalized to the absorption peak of reduced heme at 427 nm.